Low loss depressed cladding waveguide inscribed in YAG:Nd single crystal by femtosecond laser pulses

Andrey Okhrimchuk,[1,2,*] Vladimir Mezentsev,[1] Alexander Shestakov,[3] and Ian Bennion[1]

[1]*Photonics Research Group, Aston University, Birmingham B4 7ET, UK*
[2]*Fiber Optics Research Center of RAS, 38 Vavilova Street, Moscow 119333, Russia*
[3]*E.L.S. Co., 3 Vvedensky Street, Moscow 117342, Russia*
[*]*a.okhrimchuk@aston.ac.uk*

Abstract: A depressed cladding waveguide with record low loss of 0.12 dB/cm is inscribed in YAG:Nd(0.3at.%) crystal by femtosecond laser pulses with an elliptical beam waist. The waveguide is formed by a set of parallel tracks which constitute the depressed cladding. It is a key element for compact and efficient CW waveguide laser operating at 1064 nm and pumped by a multimode laser diode. Special attention is paid to mechanical stress resulting from the inscription process. Numerical calculation of mode distribution and propagation loss with the elasto-optical effect taken into account leads to the conclusion that the depressed cladding is a dominating factor in waveguide mode formation, while the mechanical stress only slightly distorts waveguide modes.

References and links

1. K. M. Davis, K. Miura, N. Sugimoto, and K. Hirao, "Writing waveguides in glass with a femtosecond laser," Opt. Lett. **21**(21), 1729–1731 (1996).
2. T. Gorelik, M. Will, S. Nolte, A. Tuennermann, and U. Glatzel, "Transmission electron microscopy studies of femtosecond laser induced modifications in quartz," Appl. Phys., A Mater. Sci. Process. **76**(3), 309–311 (2003).
3. L. Gui, B. Xu, and T. C. Chong, "Microstructure in lithium niobate by use of focused femtosecond laser pulses," IEEE Photon. Technol. Lett. **16**(5), 1337–1339 (2004).
4. A. V. Streltsov, "Femtosecond-laser writing of tracks with depressed refractive index in crystals," Proc. SPIE **4941**, 51–57 (2003).
5. S. Taccheo, G. Della Valle, R. Osellame, G. Cerullo, N. Chiodo, P. Laporta, O. Svelto, A. Killi, U. Morgner, M. Lederer, and D. Kopf, "Er:Yb-doped waveguide laser fabricated by femtosecond laser pulses," Opt. Lett. **29**(22), 2626–2628 (2004).
6. A. G. Okhrimchuk, A. V. Shestakov, I. Khrushchev, and J. Mitchell, "Depressed cladding, buried waveguide laser formed in a YAG:Nd³⁺ crystal by femtosecond laser writing," Opt. Lett. **30**(17), 2248–2250 (2005).
7. J. Siebenmorgen, T. Calmano, K. Petermann, and G. Huber, "Highly efficient Yb:YAG channel waveguide laser written with a femtosecond-laser," Opt. Express **18**(15), 16035–16041 (2010).
8. G. A. Torchia, A. Rodenas, A. Benayas, E. Cantelar, L. Roso, and D. Jaque, "Highly efficient laser action in femtosecond-written Nd:yttrium aluminium garnet ceramic waveguides," Appl. Phys. Lett. **92**(11), 111103 (2008).
9. J. Thomas, M. Heinrich, J. Burghoff, S. Nolte, A. Ancona, and A. Tünnermann, "Femtosecond laser-written quasi-phase-matched waveguides in lithium niobate," Appl. Phys. Lett. **91**(15), 151108 (2007).
10. A. Okhrimchuk, "Femtosecond fabrication of waveguides in ion-doped laser crystals," *in Coherence and Ultrashort Pulse Laser Emission*, F. J. Duarte, ed., (InTech, 2010), pp. 519–542. http://www.intechopen.com/articles/show/title/femtosecond-fabrication-of-waveguides-in-ion-doped-laser-crystals.
11. D. G. Lancaster, S. Gross, H. Ebendorff-Heidepriem, K. Kuan, T. M. Monro, M. Ams, A. Fuerbach, and M. J. Withford, "Fifty percent internal slope efficiency femtosecond direct-written Tm³⁺:ZBLAN waveguide laser," Opt. Lett. **36**(9), 1587–1589 (2011).
12. A. G. Okhrimchuk, V. K. Mezentsev, H. Schmitz, M. Dubov, and I. Bennion, "Cascaded nonlinear absorption of femtosecond laser pulses in dielectrics," Laser Phys. **19**(7), 1415–1422 (2009).

13. A. G. Okhrimchuk, V. K. Mezentsev, V. V. Dvoyrin, A. S. Kurkov, E. M. Sholokhov, S. K. Turitsyn, A. V. Shestakov, and I. Bennion, "Waveguide-saturable absorber fabricated by femtosecond pulses in YAG:Cr^{4+} crystal for Q-switched operation of Yb-fiber laser," Opt. Lett. **34**(24), 3881–3883 (2009).
14. A. W. Snyder and J. D. Love, *Optical Waveguide Theory* (Chapman & Hall, 1983).
15. R. W. Dixon, "Photoelastic properties of selected materials and their relevance for applications to acoustic light modulators and scanners," J. Appl. Phys. **38**(13), 5149–5153 (1967).
16. A. Benayas, W. F. Silva, C. Jacinto, E. Cantelar, J. Lamela, F. Jaque, J. R. Vázquez de Aldana, G. A. Torchia, L. Roso, A. A. Kaminskii, and D. Jaque, "Thermally resistant waveguides fabricated in Nd:YAG ceramics by crossing femtosecond damage filaments," Opt. Lett. **35**(3), 330–332 (2010).

Introduction

Laser inscription of waveguides by means of femtosecond (fs) pulses has shown impressive progress since its first demonstration in glasses with a femtosecond laser operating at 800 nm [1]. Several years later feasibility of waveguide inscription in crystals was also shown [2–4]. Femtosecond fabrication of waveguide lasers in glasses and crystals has a great practical importance since it facilitates manufacturing of extremely compact and reliable laser sources. The first demonstration of a femtosecond written waveguide laser was recently reported [5]. Eventually, femtosecond written waveguide lasers were demonstrated in Nd:YAG [6], Yb:YAG [7] single crystals, and also in Nd:YAG crystalline ceramics [8].

In this paper femtosecond written waveguides in crystals are classified as Stress Induced Waveguides (SIW), Depressed Cladding Waveguides (DCW), and directly written waveguides (DRW). The SIW type is formed by a modification of the refractive index due to elasto-optical coupling to mechanical stress induced in the vicinity of a fs inscribed track [2] and between the two tracks [7–9]. Both kinds of such SIWs require a low divergent or even diffraction limited pump beam in order to confine pump light inside the waveguide. The DCW type comprises of the core, which is the intact domain of a crystal, and a surrounding *depressed cladding* composed of parallel tracks with a reduced refractive index [6] whereby the mechanical stress has minor influence on the waveguide modes. A principal feature of such tracks is that there is no detectable manifestation of any irregular damage as opposed to the SIW type whereby the stress could be accomplished by some damage inside the tracks [2,9]. The DCW type features the lowest propagation loss (0.22 dB/cm [6]). Due to geometric flexibility, the cladding in DCW may consist of a fairly large number of tracks confining the flexibly large waveguide area. This feature is advantageous for coupling to multimode laser diodes [6,10]. In the DRW type waveguides, a core is formed in the bulk of crystal being directly irradiated by laser pulses. This type was originally observed in [3] and can be relatively easily fabricated in $LiNbO_3$ crystals.

In our previous paper devoted to a CW waveguide laser with depressed cladding fabricated in Nd:YAG single crystal the planar geometry was exploited [6]. In this paper we turn to the multimode depressed cladding waveguide fabricated in YAG:Nd crystal with the circular core in a pursuit of a better match of multimode fiber used to couple the laser crystal with a laser diode pump. Such an architecture has also been exploited for the Nd:YAG/Cr:YAG Q-switched microchip laser [10], and Tm:ZBLAN CW laser [11]. Since the CW regime is more sensitive to the cavity loss, we utilized this feature in the present study for precise characterization of the propagation losses in DCW with circular cross section written in Nd:YAG crystal. We also show that DCW inscribed with a beam waist of elliptical cross section exhibits record low loss among all the femtosecond written waveguides in crystals.

Fabrication of waveguides

The experimental setup used for waveguide inscription is similar to that described in our previous experiments [10,12,13]. We used a Ti:Sapphire laser system with pulse duration of 110 fs and repetition rate of 1 kHz. The principal distinguishing feature of our experimental setup is that in the plane perpendicular to beam propagation the laser beam waist has an elliptical cross section, elongated towards an inscribed track. The beam is focused by a

defocusing cylindrical lens with focal distance $f = -34$ cm and *Mitutoyo* lens with *NA* = 0.55 down below the polished surface of YAG:Nd (0.3% at.) at the depth of 70 - 170 µm. Substantial spherical aberration at the air-crystal interface occurs for greater focusing depth. It leads to elongation of the laser beam in the volume of the sample hence the density of the deposited energy is reduced. Thus the inscription threshold is remarkably higher for the depths greater than 200 µm. The crystal was moving at the speed V = 0.5 or 0.7 mm/s perpendicular to the laser beam axis, along the polarization vector. Under these conditions a single track featuring lower refractive index compared to untreated material was inscribed. Writing of single tracks in YAG: Nd(0.3%at.) has already been investigated under these conditions [10]. Figure 1 shows the dependence of the Permanent Refractive Index Change (PRICE) and the transverse size of a track parallel to the incident beam (track height) versus input pulse energy.
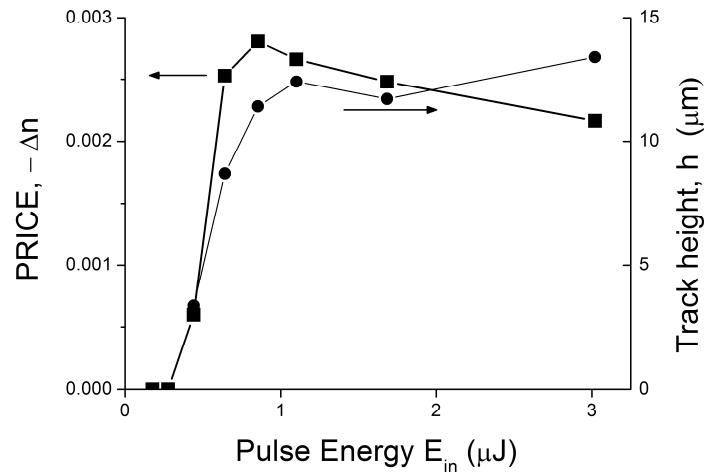

Fig. 1. Negative permanent refractive index change in Nd(0.3%at.):YAG crystal at the wavelength of 600 nm (squares) and transverse size of a track along inscribing beam (circles) versus energy in femtosecond inscription with 110 fs pulse at wavelength of 800 nm and repetition rate of 1 kHz. Scan velocity V = 0.5 mm/s. Polarization of femtosecond pulses is parallel to the translation direction. Laser beam is focused at 63 µm below the crystal surface.

Four DCWs were fabricated in the same crystal at the depth of 120 µm under the crystal surface as measured for DCWs centers. The crystal surface was parallel to the (100) crystallographic plane, and the waveguides were parallel to the [010] crystallographic axis with the accuracy of 5 degrees. The track geometry is shown in Fig. 2. The waveguide clad consists of a chain of tracks forming a tube. The number of tracks in the tube was of 54 or 66 (see Table 1) depending on the design. Outer arrays of 3 tracks on the right and left sides were inscribed to reinforce thin walls of the cladding in those positions and to diminish the mode leakage. The waveguides were slightly elliptical with vertical diameter of 116 µm (parallel to incident beam), and horizontal diameter of 110 µm. Waveguide center was at the depth of 120 µm under the crystal surface. The main inscription parameters are summarized in Table 1. We used pulse energies in the range of negligible dependency of PRICE and the track size upon the pulse energy in order to achieve better reproducibility and uniformity of refractive index change (Fig. 1). Thus the magnitude of PRICE in the DCW is typically 0.0025 while the track height was of 12 µm.
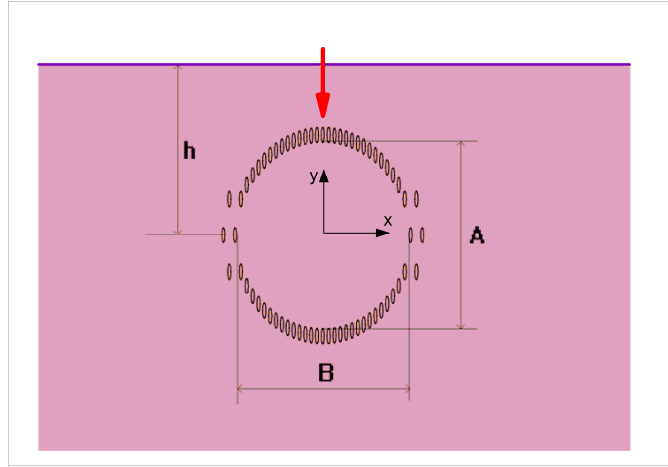
Fig. 2. Scheme of a waveguide consisting of 66 tracks. End view. Waveguide sizes: A = 116 µm, B = 110 µm, depth of waveguide center h = 120 µm. The red arrow indicates the propagation direction of inscribing beam.

After inscription, the sample was cut in two pieces of 11.4 and 8.1 mm length. Ends of the waveguides were polished, and nearly 200-µm crystal layers containing improperly inscribed tracks ends were removed. Waveguide end facets and the inscribed tracks were made orthogonal with the accuracy of 10 min. Antireflection dielectric coating for 1064 nm was applied to both ends of the 11.4 mm long sample, and the sample of 8.1 mm length was supplied with the same antireflection dielectric coating on one end, and also with a dichroic mirror on the other end. The dichroic mirror has 100% reflectivity at oscillation wavelength of 1064 nm, and transmits 98% at pump wavelength of 809 nm.

Pump light waveguiding

A fiber coupled laser diode was used for pumping in the oscillation experiments. The fiber has a core diameter of 105 µm and numerical aperture *NA* of 0.15. The fiber was winded in two orthogonal planes to ensure unpolarized pump light. Two alternative schemes for coupling pump diode with a waveguide were used. In the first scheme two achromatic lenses with focal length of 3.3 mm each project an image of output end of pumping fiber at the input facet of one of the 11.4 mm long waveguide as seen in Fig. 3(a). Magnification was optimized for the best match between the core diameters of fiber and the DCW in crystal. A dichroic HR mirror was attached to the pumping end. The second scheme utilizes a simple butt-coupling into waveguides in 8.1 mm long sample as shown in Fig. 3(b).
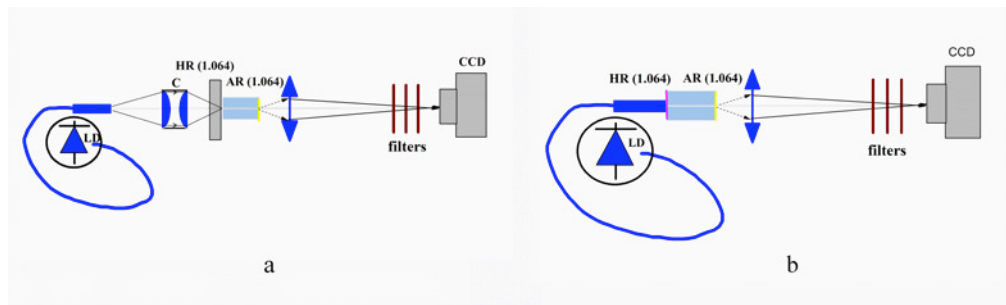

Fig. 3. Pump light propagation loss measurements. (a) Pump light is coupled through lenses. (b) Butt-coupling.

We made measurements in order to estimate and compare pumping efficiencies of all the inscribed waveguides in both pumping schemes. A microscopic lens with $NA = 0.2$ was used to collect light emitted from the opposite ends of a waveguide and to transmit it to CCD camera through neutral density filters and a color filter rejecting luminescence emission originating from Nd^{3+} ions and passing the pump light. Position of the microscopic lens was tuned in such a way that it projects an image of the output waveguide end to the CCD matrix with magnification of about ten. The power of the pump light going from the waveguide is measured in "aperture" regime built in camera software. The power is measured in the aperture exactly matched to the waveguide end image. In order to extract propagation loss this power was normalized to that passed through unperturbed region of the crystal, when the pump light is focused onto the crystal facet far from waveguides and the microscopic lens projects an image of this facet on the CCD. Propagation losses measured in this way are summarized in Table 1. In this procedure coupling loss is included in propagation loss shown in the table. This is the reason why the propagation loss for the first coupling scheme is higher than that for the butt-coupling scheme for all waveguides. It is obvious that coupling loss is higher in the first case as it was technically difficult to build an image of pumping fiber on the input facet with magnification exactly equal to unity. We believe that coupling loss in the case of butt-coupling is negligible as alignment is straightforward as the core fiber diameter is matched to the waveguide core diameter. Thus the last column of Table 1 represents propagation loss.

Table 1. Inscription Parameters and Attenuation Coefficients of Pump Light for 11.4 mm Waveguides

No. of waveguide	Total number of tracks in clad	Energy per pulse E_{in} (µJ)	Sample velocity V (mm/s)	Pump attenuation coefficient (cm^{-1})	
				Pump through the lens	Butt-coupling
1	66	1.5	0.5	1.54	1.12
2	66	1.2	0.5	**1.42**	**1.10**
3	54	1.4	0.5	1.80	1.28
4	54	1.5	0.7	2.38	1.84

Analysis of data presented in Table 1 leads to the conclusion that propagation loss does not depend upon inscription pulse energy E_{in}, that is for the input pulse energy range used for waveguide inscription no additional scattering loss depending on the inscription pulse energy is observed (see waveguides #1 and #2 for comparison). The loss is remarkably higher for waveguides 3 and 4. It is obviously due to i) sparser spacing of tracks in the cladding (55 tracks versus 66), ii) lower PRICE in waveguide 4 due to higher inscription speed. Absorption coefficient for the laser diode pump light measured in the region far from waveguides was found to be 1.2 cm^{-1}. Thus, nearly 50% of pump energy is absorbed by Nd^{3+} ions in a waveguide core when waveguides No.1 and 2 are pumped in butt-coupling scheme.

Oscillation experiments

CW oscillation at 1064 nm was obtained and investigated for both pumping schemes. Lasing in all waveguides was achieved by adding output coupler to the right end of waveguide in the schemes shown in Fig. 3. The first scheme (Fig. 3(a)) allowed to reach lower cavity loss compared to that in the second scheme (Fig. 3(b)), because in the former case both mirrors could be tuned, and maximal coupling of a reflected mode to the same counter propagating mode can be obtained. This is not the case in the second scheme, where HR mirror is fixed on the crystal facet. In this case considerable loss arises from lowered back coupling of oscillating mode in the reflection stage because of the deviation of the angle θ between crystal facet and waveguide axis. Coupling efficiency of Gaussian beam entering waveguide from

free space with Gaussian waveguide mode can be expressed as function of an incident angle θ [14]. Loss on reflection stage can be calculated as

$$\frac{P_c}{P_{on}} = \exp\left(-8\left(\frac{\pi r_0 n\theta}{\lambda_0}\right)^2\right),$$

(1)

where P_c is back coupled power, P_{on} is power of a beam falling on a mirror, r_0 is radius of the mode at $1/e$ level of intensity, λ_0 is wavelength in vacuum, n is the refractive index. We failed to reduce the deviation angle θ to less than 10 angular minutes in the polishing process. Consequently, the effective reflectance should be expected as low as 55% according to Eq. (1). Indeed higher oscillation thresholds and lower slope efficiencies were obtained for the second scheme. However, the effective reflectance in our experiments is probably somewhat higher than that predicted by Eq. (1) because in case of multimode waveguide incoming beam couples to a few modes.

Waveguide #2 showed the highest efficiencies among the investigated waveguides. This is not surprising since according to Table 1 this waveguide demonstrated the lowest propagation loss for pump emission. The results of measurements of output power versus pump power for this waveguide in the first scheme and for different transmittance of output coupler are presented in Fig. 4. The highest output power and slope efficiency were obtained for the output coupler with T_{OC} = 25%, when the slope efficiency was as high as 23%. Optimal optical-to-optical slope efficiency in the second pumping scheme was found to be slightly lower at 19.5%. However efficiency in optical output – pump current coordinates was even higher for the second scheme. For example, we obtained 150 mW and 180 mW at the outputs for the first and second schemes correspondingly at the same pump current of 2.0 A. This is explained by more efficient pump coupling in the second scheme.
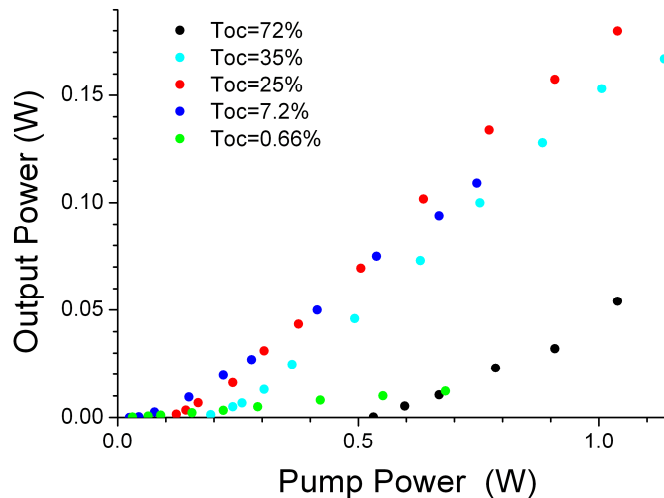

Fig. 4. Dependences of output CW oscillation power upon input pump power for waveguide No.2 with different output couplers. Pump scheme is shown in Fig. 3(a).

We have applied Findlay-Clay analysis to estimate inter-cavity loss of the waveguide laser based on Waveguide 2. Dependence of the input pump power at the threshold upon output loss was obtained with data of Fig. 4. The results are presented in Fig. 5. The solid line approximates dependency in the region of high reflectance of output couplers. The whole experimental dependence deviates from linear; that is threshold pump power increases super-

linearly with logarithmic output loss. We suggest that it is related to the increased contribution of super luminescent relaxation of the inversion population at the lower output coupler reflectance, as gain is higher in this case. Intersection of the approximating line with horizontal axis gives a round trip loss in laser cavity, which is found to be 0.063. Assuming that all round trip losses are due to propagation loss, we obtain that propagation loss is as high as 0.12 dB/cm. As a matter of fact this value should be considered as upper limit, because part of the round trip loss is probably due to non-ideal reflectance on the mirrors.
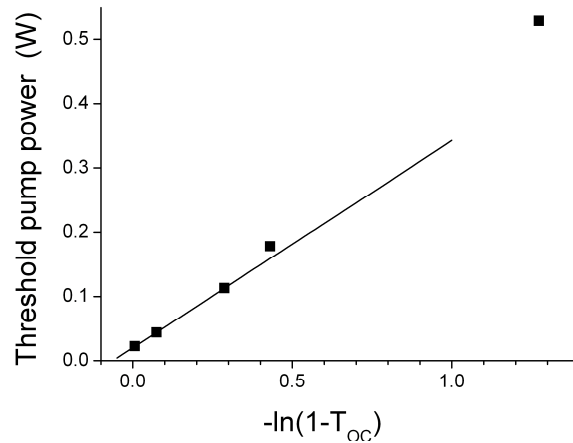

Fig. 5. Findlay-Clay analysis for waveguide laser No.2 with external mirrors. Dependency of pump power at the threshold upon output loss. Solid line is a linear approximation made for region of low output coupling.

The near field distribution for oscillating modes at the output coupler was measured. The images were obtained on a CCD camera with microscopic lens of $NA = 0.2$, similar to schemes shown in Fig. 3. Optical magnification was of 10. Colour glass IR filters were used to reject pump emission, neutral density glass filters attenuated laser beam. It was found that mode field distribution i) is sufficiently different in both investigated pumping schemes, ii) slightly varies for different waveguides, iii) depends upon transmittance of output coupler. In the first scheme we observed that mode field distribution varies with tuning of incident angle and spot size of the pump light. A smooth near field distribution with one maxima was obtained only in the cavity with low transmittance of the output coupler ($T_{OC} = 0.66\%$) as displayed in Fig. 6. We assumed that the near field image obtained at the output of Waveguide #2 with high reflectance output coupler corresponds to the fundamental mode of this waveguide, as the picture does not change in the whole investigated range of pump power. This is illustrated in Fig. 7, where horizontal and vertical diameters of the distribution in dependency upon input pump power are presented and constant sizes of the intensity distribution are confirmed.

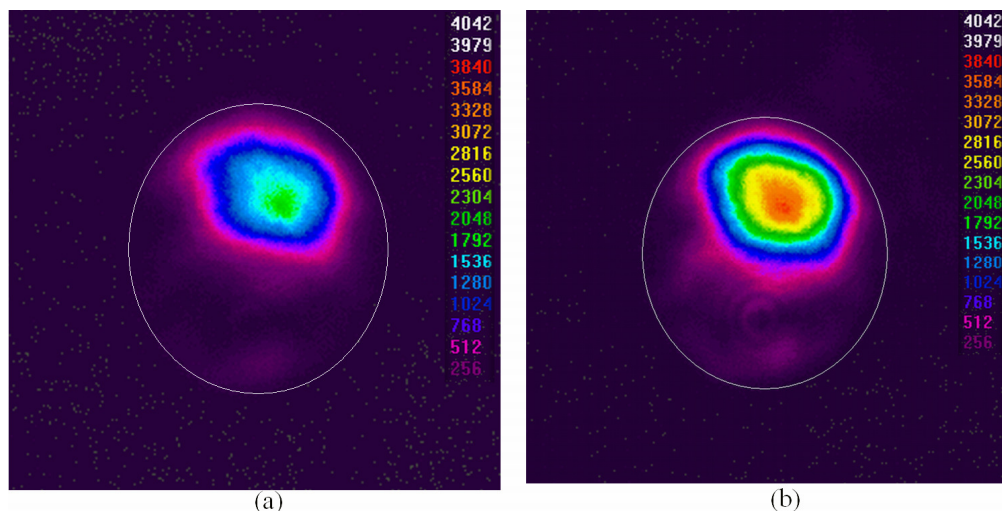<div align="center">(a)   (b)</div>

Fig. 6. Near field images of output waveguide laser light. Thin solid line designates inner elliptical boundary of the cladding with vertical A and horizontal B diameters of 116 and 110 µm correspondingly (Fig. 2). Pump is coupled through lenses; and cavity is comprised by external mirrors. Transmittance of output coupler T_{oc} = 0.66%. (a) Pump power is slightly above threshold P_{pump} = 28 mW. (b) Pump power is strongly above threshold: P_{pump} = 551 mW.
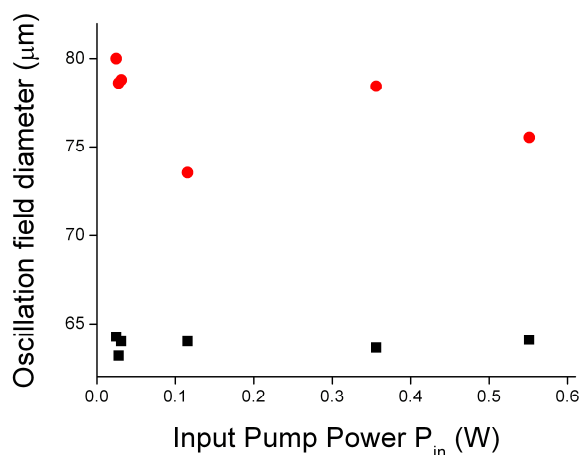

Fig. 7. Dependence of vertical (black square) and horizontal (red circles) oscillation field diameters (at the level of $1/e^2$ of intensity) in dependency upon input pump power for Waveguide #2 and output coupler with transmittance T_{OC} = 0.66%. Cross-section distribution of oscillation intensity was analyzed by D4-sigma method

Field distribution fills the whole waveguide aperture and has numerous maxima in the cavity with low reflectance output coupler, which means multimode regime of oscillation.

Mechanical stress and refractive index perturbation

Mechanical stress is the main mechanism for waveguiding in the case of SIW type waveguides. In this section, we show that in the case of DCW stress is not primary factor for waveguiding although femtosecond inscription produces some mechanical stress around the inscribed tracks too. The last fact is illustrated by the observed induced birefringence inside and around the waveguide. Figure 8 shows microscopic image of the end view of Waveguide #2. The picture was captured for light transmitting through two crossed polarizers with the

waveguide positioned between them. Two vertical stripes above and beneath the circular waveguide structure are cracks indicating significant induced mechanical stress locked during the inscription process in the crystal. The cracks developed during polishing while there were no cracks just after the inscription. It is important and interesting to estimate contribution of stress induced refractive index perturbations to the DCW formation.
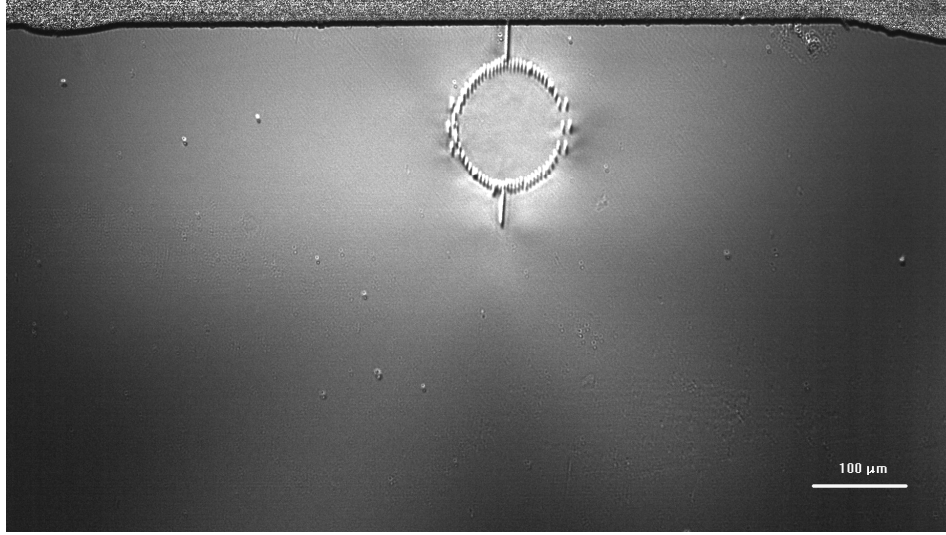

Fig. 8. End microscopic views of the Waveguide #2 for sample placed between crossed polarizers.

We performed numerical analysis of the waveguide modes considering that mechanical stress around and inside waveguide developed from some initial pressure p_i generated inside each track due to structural changes resulting from exposure to femtosecond laser pulse. Such pressure is a phenomenological characteristic accounting for all the mechanical effects produced by femtosecond pulses. We consider an approximation of instantaneous generation of the initial pressure in a track due to substantial difference in temporal scales of laser plasma recombination and eventual elastic relaxation of crystal media in the vicinity of the tracks. Negative pressure causes compressive stress inside a track, and positive pressure causes tensile stress.

Relaxation deformation is the origin for refractive index change outside of tracks. 2D distribution of refractive index tensor $n_{i,j}$ was calculated according to formulas written in the approximation of small strains ($u_{ii} << 1$):

$$n_x = n_{YAG}\left(1 - 0.5n_{YAG}^2\left(p_{11}u_{xx} + p_{12}u_{yy}\right)\right)$$
$$n_y = n_{YAG}\left(1 - 0.5n_{YAG}^2\left(p_{11}u_{yy} + p_{12}u_{xx}\right)\right), \qquad (2)$$
$$n_{xy} = n_{yx} = -0.5n_{YAG}^3 p_{44} u_{xy}$$

where n_{YAG} is refractive index of unperturbed YAG crystal (n_{YAG} = 1.82), n_x and n_y are perturbed refractive indexes for respective polarizations, and n_{xy} is an index responsible for depolarization of pure "x" or "y" field components, $u_{i,j}$ is strain tensor, $p_{i,j}$ is elasto-optical tensor in a vector form (for YAG p_{11} = −0.029, p_{12} = 0.0091, p_{44} = −0.0615 at 633 nm [15]). Representative results of these calculations are presented in Fig. 9, where distribution of refractive index perturbations $\Delta n_x = n_x\text{-}n_{YAG}$ and $\Delta n_y = n_y\text{-}n_{YAG}$ along main waveguide symmetry axes ("x "and "y" in Fig. 2) is shown.

Commercial Comsol Multiphysics software (version 3.5) was used to perform numerical calculations. Basic drawing for model waveguide is shown in Fig. 2. Cross section of each track was approximated by ellipse with axes of 2 and 9 µm and uniform PRICE inside a track of −0.0025. Refractive index distribution outside the tracks was calculated considering elastic deformation of YAG crystal. Additionally to the basic drawing two empty splits in crystal body each of 1 µm wide and 40 and 36 µm long were accepted in the model to simulate cracks shown in Fig. 8.

Simulations were performed in two steps. In the first stage structural mechanics module of Comsol was implemented to calculate 2D stress and strain distributions in a plane of waveguide cross section. We have found that the stress locked inside the track is lower than initial pressure due to relaxation deformation. It is sufficiently anisotropic with major "y" component and minor "x" component. There is a slight variation in the stress components depending on the track location in DCW structure. This is obviously caused by superposition of stress field from different tracks. Average relaxation factor of 2 with maximal deviation of about 20% was found for the "y" stress component, and the "x" component is less than the initial pressure by factor of nearly 10. It should be noted that parallel to tracks "z" stress component remains equal to the initial pressure p_i, but corresponding strain u_{zz} is zero and has no impact on refractive index perturbations. It is consistent with the fact that the track length is much larger than its cross-section dimensions. Thus stress inside tracks averaged among directions in "x-y" cross section plane and among all tracks σ_{av} is an adequate parameter to characterize the impact of deformations on refractive index. We note for reference that $\sigma_{av} = 0.25\, p_i$ in our geometry.

The calculation revealed that refractive index distribution n_x and n_y along "x" axis is symmetrical relatively waveguide center as expected. This is not the case for index dependences upon coordinate "y". The reason for such behavior is the vicinity of crystal surface, which breaks mirror symmetry relatively "x" axis. In other words the picture of stress relaxation below waveguide is differed from the picture above because of lack of crystal body at a distance 120 µm and higher from the waveguide center.
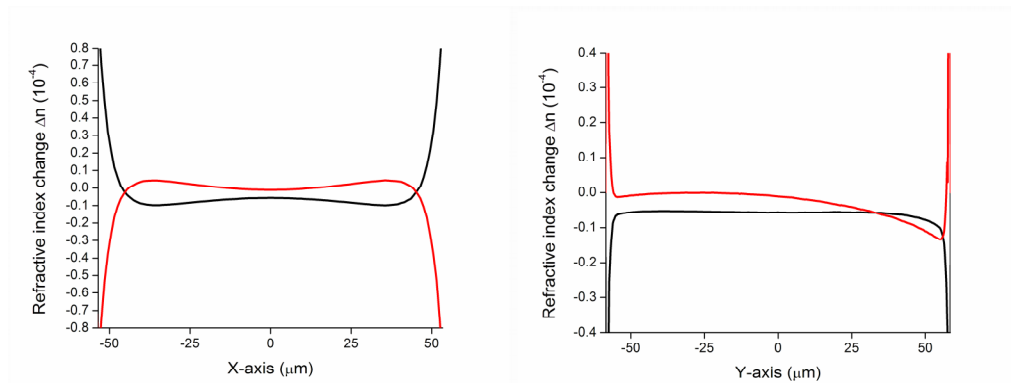

Fig. 9. Distribution of refractive index change inside waveguide core induced by compressive stress inside cladding tracks along two orthogonal axes of symmetry as seen in Fig. 2. Black solid line is for horizontal "x" polarization, and red solid line is for vertical "y" polarization. σ_{av} = −0.5 GPa.

In the second stage of numerical modeling, Comsol full vectorial Maxwell mode solver was set to solve 2D eigenvalue problem to find propagation constant (effective refractive index) of the fundamental mode of the model waveguide with refractive index distribution in the core and outside the cladding calculated according to Eqs. (2). Refractive index in the tracks was taken as n_{YAG} −0.0025 according to the results presented in Fig. 1. The perfectly

matched layer (PML) technique was implemented to suppress outer cladding modes having no relation to waveguides in consideration. Squire PML with inner size of 500 µm was used.
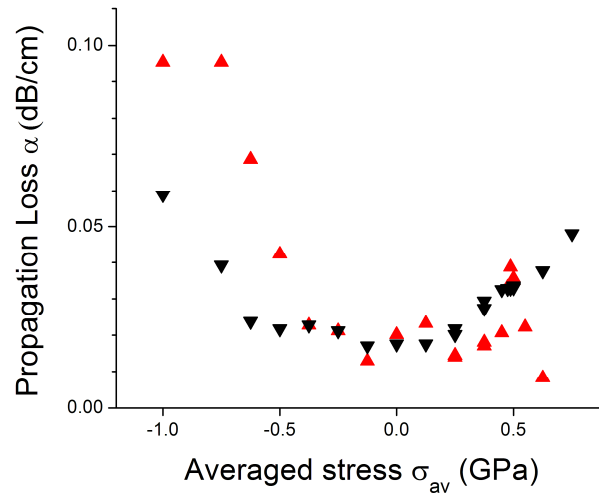

Fig. 10. Calculated dependences of waveguide propagation loss upon averaged stress inside tracks for fundamental modes of horizontal (red up-triangle) and vertical (black down–triangle) polarizations.

Fundamental mode of the model waveguide with uniform distribution of refractive index among the core ($\sigma_{av} = 0$) has a perfect axial symmetry with peak intensity located at the waveguide center and diameter of 80 µm. Further mode analysis has shown that fundamental mode is distorted, that is the peak of intensity splits into two maxima when compressive stress exceeds 0.75 GPa, or tensile stress exceeds 0.5 GPa. There are two fundamental modes with ellipticity less than 0.4 and average diameter close to 80 µm for the pressure range between these two reference points. We calculated propagation losses for first two fundamental modes of different polarizations as an imaginary part of the effective refractive index in dependency upon averaged stress in track σ_{av} (Fig. 10). Neither mode distortion nor remarkable change in waveguide propagation loss was found for the relatively low stress in the range between −0.25 GPa to 0.25 GPa.

Earlier spectroscopic investigations [16] gave the evidence of residual compressive stress inside a track written in ceramic Nd:YAG. The magnitude of this stress was estimated then as high as 0.4 GPa. We suggest that the sign of stress in our tracks is also negative, and the magnitude of frozen stress in our case does not seem to be sufficiently higher than that described in [16] since we used slightly lower femtosecond pulse energy while the beam waist had nearly the same cross section area. This conclusion is supported by the fact that we observed a fundamental mode with a single maximum in the oscillation experiments, which is only possible for magnitude of the averaged stress σ_{av} less than 0.75 GPa according to the numerical solution of the eigenvalue problem. However the averaged stress magnitude should be higher than 0.25 GPa as the mode ellipticity was observed (Fig. 6, 7). Thus the initial compressive stress in the tracks is expected to be in the range of 0.25-0.75 GPa, which is consistent with the results of [16].

Discussion

Refractive index change induced purely by stress in waveguide core peaks near the tracks and its magnitude rapidly decays towards the waveguide center (Fig. 9). At the points with maximum stress the induced refractive index change is lower than refractive index change

inside the tracks produced by direct femtosecond exposure due to structural changes at least by the factor of 3. At the center of waveguide it is more than a factor of 250 lower than inside the tracks. These considerations together with numerical evidence of small influence of mechanical stress on mode behavior lead to the conclusion that stress does not play significant role in DCW fabrication, and depressed cladding is a dominating factor in waveguide mode formation.

DCWs described in this paper exhibit record low loss in comparison with SIWs, often being written in YAG and other crystals, where loss exceeds 0.5 dB/cm. We consider that there are two reasons for this, both connected with more regular and smooth tracks inherent to the DCW type. The first reason is directly linked with the femtosecond beam waist of an elliptical cross section, which rises self-focusing threshold in comparison with traditional beam of axial symmetry. Such inscription method leads to a better control over the energy deposition and waveguide inscription process [12]. The second reason is that the density of the absorbed energy in case of DCW is at least an order of magnitude lower compared to SIW since in the former case there is no need to produce wide spreading stress outside the tracks. Indeed, pulse energy for SIW inscription in YAG [7,8] is nearly the same or even higher than for DCW inscription (this and [6]), while area of elliptical beam waist is an order of magnitude larger than for the traditional axially symmetric beam waist, because both waists are produced by lenses with similar *NA*s of around 0.5, and for formation of elliptical beam waist a long distance focus cylindrical lens is additionally included in the setup, which elongates traditional circular waist by factor of about 10 in direction that is transverse to that of beam propagation. Number of accumulated pulses in a point of a track is nearly the same for both techniques (nearly of 20).

It is possible to further improve quantitative agreement between the numerics and the experiments in describing mode field distribution by more accurate account of elasto-optical coupling and pump distribution. However the model described above already provides a good first approximation. Realistic stress clearly hits the range of plastic deformation and even that of the material failure. Indeed the initial pressure p_i of a few GPa is about 1% of the Young modulus for YAG crystal (280 GPa). Deformation of such magnitude is typical in creation of moving dislocations in crystals which means that the inscription can take place beyond the elastic limit even outside the tracks. Having said that, the numerics clearly explain the distortion of fundamental mode by the relative vicinity of crystal surface. Hence the circular distortion could be rectified by inscribing the whole waveguide structure deeper under the surface while the mirror asymmetry can be eliminated by accurate placing of the waveguide symmetrically between the crystal surfaces. Another way of cardinal eliminating of the distortions is a heat treatment [16].

Conclusion

Tube-like architecture of depressed cladding waveguide is naturally suited for microfabrication by femtosecond laser inscription by a beam with an elliptical cross section in the plane perpendicular to the incidence direction. It allows manufacturing of efficient ultra compact solid state waveguide lasers on the basis of YAG:Nd crystal with very low propagation loss. Such architecture allows pumping laser cavity with widely available multimode laser diodes using direct butt-coupling.

Mechanical stress accompanying the inscription process does not play a substantial role in DCW formation, but detrimentally affects refractive index distribution inside unexposed core and in combination with non-uniform pump light distribution undesirably distorts the waveguide modes. It results in lower oscillation efficiency and output beam quality. The detrimental effects of the locked stresses can be mitigated by allocating the waveguide structure symmetrically between the surfaces.